JOURNAL OF GEOPHYSICAL RESEARCH, SPACE PHYSICS VOL. 75, NO. 31, NOVEMBER 1, 1970

Whistler Duct Properties Deduced from VLF Observations Made with the Ogo 3 Satellite near the Magnetic Equator

JACYNTHO J. ANGERAMI

Radioscience Laboratory, Stanford University, California 94305

While the great majority of ground whistlers are interpreted as indirect evidence of magnetospheric ducts, the first direct evidence of ducts was obtained from the Stanford University broadband VLF experiments on Ogo 1 and Ogo 3. Five discrete whistler ducts were encountered by Ogo 3 on the inbound pass of June 15, 1966, between $L = 4.7$ and 4.1. Each duct was characterized by reception at the satellite of ducted whistlers with a distinct spectral shape, and of the high-frequency portions of whistlers (leakages) that propagated inward from outer ducts. The data were interpreted in detail by ray tracing in a model magnetosphere that includes ducts of enhanced ionization. The following conclusions resulted: (1) the L shell thicknesses of the observed ducts ranged between 0.035 and 0.070 earth radii, and the interduct separations ranged between 0.017 and 0.18 earth radii; (2) the dimension of the ducts in longitude was estimated to be of the order of 4°, or 0.3 earth radii at the equator, which is a factor of ~4–8 greater than the L shell dimension; (3) the whistler ducts are much more likely to be enhancements than troughs; (4) the minimum enhancement factors needed to trap frequencies up to half the equatorial electron gyrofrequency are on the order of 8%, with smaller values producing upper cutoffs at lower frequencies; (5) the limited spreading of the calculated leaked rays is in general agreement with the corresponding regions of observation and relative signal amplitudes; (6) the low cutoffs of leaked signals are probably due to accessibility; (7) cyclotron and Landau interactions are likely to play a role in upper cutoffs of leaked signals; (8) the upper cutoff of ground whistlers near $f_{H0}/2$ is a trapping (rather than absorption) effect; (9) the hydrostatic type of distribution of ionization along the field lines is applicable in the plasmasphere; and (10) the travel times (and frequency of minimum delay) of ducted whistlers can be calculated with good accuracy by assuming purely longitudinal propagation.

Since 1956, there has been a steady accumulation of indirect evidence for the existence of magnetospheric whistler ducts, field-aligned structures (presumably tubes of enhanced ionization) capable of guiding whistler waves between conjugate hemispheres. Until a recent report based on Ogo 1 VLF whistler data [*Smith and Angerami*, 1968], however, there was no in situ evidence that such ducts actually exist. The Ogo 1 report showed evidence of whistler spectra whose properties changed discretely as a series of ducts was encountered.

Ogo 3 data have provided a similar but much more elaborate example of in situ duct observations, thus making possible the present study of several of the properties of ducts, including high-frequency leakage from ducts, enhancement factors, duct size, etc. These topics have in the past been the object of much speculation and in some cases, considerable controversy.

Propagation of whistlers in ducts of enhanced ionization was investigated by *Smith* [1961], who demonstrated the validity of using the strictly longitudinal approximation to calculate travel times. He also predicted an upper cutoff in ducted whistler components at half the minimum electron gyrofrequency along the path. This cutoff is due to the untrapping of waves at frequencies above half the local gyrofrequency f_H. The untrapping is due to a fundamental change in the anisotropy of the medium at $f_H/2$. Ground whistlers do in fact exhibit an abrupt upper intensity cutoff (the wave intensity drops by 10 db or more within a fraction of a kilohertz). *Liemohn and Scarf* [1964] have interpreted this effect as the result of thermal damping in the magnetosphere, but a recent empirical study showed the effect to be consistent with the half-gyrofrequency propa-

gation effect predicted by Smith [*Carpenter*, 1968]. (More recent theoretical studies of the cyclotron resonance [*Liemohn*, 1967] and Landau [*Kennel and Thorne*, 1967] interactions that account for suprathermal electrons are discussed in a later section.)

The problem of identifying the appropriate mechanism for the upper cutoff involves the model of the fieldline distribution of ionization in the magnetosphere. Recent ground-based whistler studies strongly support use of a hydrostatic model [*Angerami and Carpenter*, 1966; *Angerami*, 1966], rather than a more rapidly varying gyrofrequency model ($N_e \propto R^{-3}$) proposed in earlier work. When the hydrostatic model is used in calculations with ground whistler data, the observed intensity cutoff is found to be at $\sim 0.5\ f_{H0}$ (f_{H0} is minimum gyrofrequency along path) instead of $\sim 0.6\ f_{H0}$ as in the case of the R^{-3} model.

In this paper the first direct evidence on the nature of ducting is reported, based on in situ whistler observations made by the Ogo 3 satellite. The interpretation of the data strongly supports both the theoretically predicted cutoff at $0.5\ f_{H0}$ and the hydrostatic model of magnetospheric ionization. For the cases studied it is found that the over-all thermal damping is not an important process near half the local gyrofrequency. The data lead to estimates of the L shell thicknesses of whistler ducts, their elongation or extent in longitude, and minimum enhancements needed for trapping. The data also confirm the validity of using the longitudinal approximation to calculate travel times and nose frequencies of ducted whistlers. Finally, the data give further evidence that whistler ducts are indeed enhancements, rather than depressions, of ionization.

Experiment

The Ogo 3 satellite was launched on June 7, 1966, into a highly eccentric orbit initially with perigee at an altitude of 295 km, apogee at 122,220 km, period of 48 hours and 37 min, and inclination of 30.92°. Among several experiments carried aboard Ogo 3 was a Stanford University/Stanford Research Institute VLF experiment similar to that carried by Ogo 1 [*Rorden et al.*, 1966]. The experiment consists of one broadband receiver and three narrowband sweeping receivers, all fed from a 2.9-meter diameter, 1-turn loop antenna. This paper uses data from the broadband VLF receiver (0.3–12.5 kHz), which has an instantaneous AGC action provided by a logarithmic amplifier followed by a limiter, designed to compress an 80-db dynamic range at the input into a 20-db range at the output. The net effect is that a strong signal may suppress a simultaneous weak one. The output of the broadband receiver phase-modulates a 400.85-MHz carrier (special purpose telemetry channel). At the ground the telemetry signal is demodulated, and the resulting VLF spectrum is analyzed by a Rayspan with 420 filters in a 10.5-kHz range, thus producing frequency-time spectrograms of the type illustrated in Figures 4–9.

Predicted Aspect of the Data

As a basis for later discussion of the actual data, Figure 1 shows a descriptive model of trapped waves observed by a satellite crossing magnetospheric ducts. The sketch of Figure 1*a* indicates a portion of an inbound pass of a satellite in the northern hemisphere. The dipole field lines shown represent the centers of two ducts of enhanced ionization. A lightning impulse is shown near the northern feet of the ducts. Portions of the whistler-mode waves excited in the ionosphere are trapped in the ducts and propagate upward. At frequencies lower than half the local gyrofrequency, the wave normal executes small oscillations around the direction of the geomagnetic field, and the ray describes a snakelike path along the duct. Typical ray paths of this kind are sketched for a frequency f in Figure 1*a*, where the wiggles are exaggerated for clarity. The corresponding whistler received on a satellite at S_e in the outer duct has the frequency-time spectrum sketched in Figure 1*b*.

We now consider propagation along the outer duct at a higher frequency, f', which equals half the gyrofrequency at a point A, Figure 1*c*. Because of the change in anisotropy or shape of the refractive index surface, there is no trapping beyond this point; that is, the mechanism that rotates the wave normals back in the direction of the field is no longer operative [*Smith*, 1961]. Mainly because of the curvature of the magnetic field lines, the wave normal tends to lag behind the field and to

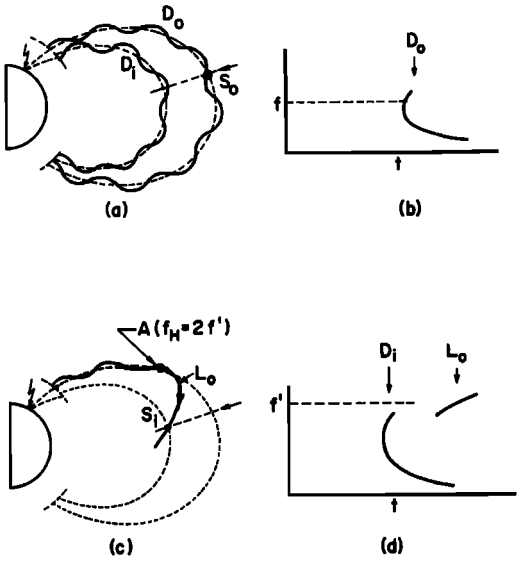

Fig. 1. Sketches to illustrate the inward leakage of whistler mode signals at frequencies above half the gyrofrequency. Section *a* represents ray paths for a frequency f less than half the gyrofrequency throughout the paths. A satellite at S_o in the outer duct receives a whistler whose frequency-time spectrum is shown by D_o in (*b*). In section *c* the curve L_o is the ray path followed by a leakage from the outer duct, at a frequency f' that equals half the local gyrofrequency at point A. A satellite at S_i in the inner duct receives both the ducted whistler D_i and the leakage from the outer duct L_o, as shown by the frequency-time spectrum in (*d*). Note that at S_o in the outer duct the satellite does *not* receive any leakage from the inner duct (see sections *a* and *b*).

point outward. Because the ray direction is given by the normal to the refractive index surface and this is now chalice-shaped [*Helliwell*, 1965], the packet of energy travels inward, as indicated by the ray L_o ('leakage from the outer duct') in Figure 1*c*. The corresponding signal received on the satellite at S_i has the frequency-time spectrum shown by the rising tone labeled L_o in Figure 1*d*. If the satellite is in a duct (as illustrated in Figure 1*c*), it may also receive a whistler produced by ducted propagation along that duct (D_i) (and initiated by the same lightning impulse that produced L_o). This whistler has higher nose frequency and shorter travel time than D_o of Figure 1*b* because of higher gyrofrequency and shorter path, respectively.

The data presented in the next section may be understood by referring to the sketches of Figure 1. Results of a detailed ray tracing that corroborate the present interpretation are shown in a later section. Inward leakages from ducts of enhanced ionization at frequencies above half the gyrofrequency have also been predicted by the ray tracings of *Cerisier* [1967].

Description of the Data

Figure 2 shows a portion of the June 15, 1966, inbound pass of Ogo 3 in a magnetic meridian plane projection. The data relevant to this paper were received near local midnight and under quiet magnetic conditions ($Kp \sim 1$ for 2 days). In the 16-min interval from 0432 to 0448 UT, the satellite moved from dipole coordinates $\theta = 9.1°$N, $L = 4.76$, to $\theta = 6.5°$N, $L = 4.08$, while keeping a nearly constant geographic longitude (47.4°W ± 0.2°). (The 'dipole coordinates' used here were obtained by following the field line defined by the *Jensen and Cain* [1962] coefficients from the satellite to the point of minimum field intensity. The geocentric distance of this point in earth radii is taken as 'L,' and the angular separation to the satellite position is the 'dipole latitude

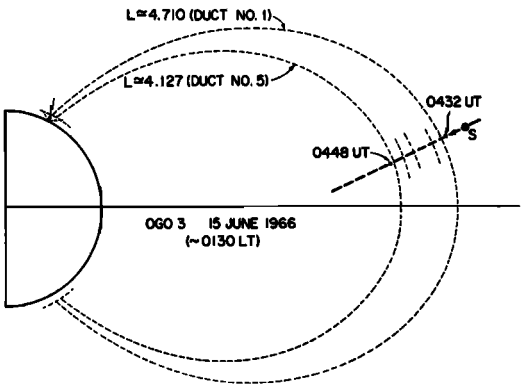

Fig. 2. Meridian cross section of the magnetosphere drawn to scale to show a portion of the inbound pass of the Ogo 3 satellite (S) relevant to this paper. The dipole field lines represent the centers of the observed ducts 1 and 5. The three intervening segments crossing the orbit show the positions of the other ducts observed, numbers 2, 3, and 4. A lightning flash in the northern hemisphere is shown, representing the sources of the whistlers described in the text.

θ.' In the ray tracing calculations described later, the field intensity of the dipole model used was chosen to match the magnetic field measured at the satellite.)

The map of Figure 3 shows the positions of the subsatellite points and the northern feet of the field lines passing through Ogo 3 in the period of interest. The corresponding southern feet of the field lines are near 72°S over Antarctica. (Because this region has low lightning activity during winter, whistlers originating in the southern hemisphere were neither expected nor observed in the present data.) The map also indicates lines of constant latitude and constant longitude for a centered magnetic dipole. The Ogo 3 data described here were telemetered to the NASA station at Rosman, North Carolina (identified as *ROS* on the map), where VLF ground data were simultaneously recorded on the same magnetic tape as the satellite data. These ground data proved invaluable in the identification of the lightning sources for the whistlers studied.

Figures 4 through 9 show time-frequency spectrograms of data from the broadband VLF receiver aboard Ogo 3. The origin of the time scale corresponds to the instant of occurrence of the lightning impulse that produced the first event shown. The vertical scale on each record represents frequency in the range 0–10 kHz. A time code generated at the Rosman telemetry station is shown by the second marks near zero frequency. Just above the time code signals, at the frequency indicated by *GR* on the right, we have inserted a narrowband portion of the VLF data near a center frequency of 2.5 kHz recorded on the ground at Rosman. In this band the lightning impulses are displayed as somewhat ill-defined dots. The horizontal lines on the spectrograms are the output of the Ogo 3 rubidium vapor magnetometer (and harmonics), which utilizes the same telemetry channel as the broadband whistler data. The distance between adjacent lines is $f_H/4$, one-fourth of the electron gyrofrequency at the satellite (Heppner, private communication). The f_H line is indicated at the right of the records.

As the satellite moved inward, the spectral shapes of the observed whistlers changed discretely, in a manner consistent with guided propagation along distinct field-aligned ducts that were successively traversed by the satellite. Figure 4*a* shows the first whistler received

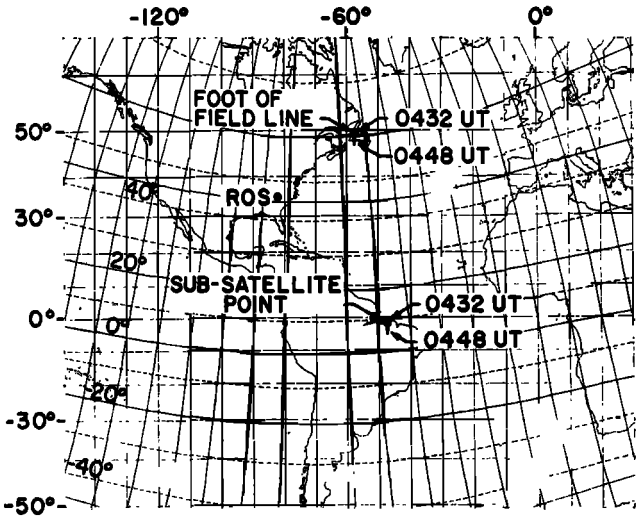

Fig. 3. World map showing lines of constant latitude and constant longitude in the centered magnetic dipole. The subsatellite points and the northern feet of the corresponding field lines for the period of interest are indicated. The latter were found by using the *Jensen and Cain* [1962] field. The southern ends of the field lines lie off the limits of the map. Note the proximity between the northern feet of the field lines and the Rosman telemetry station, where VLF ground signals were recorded simultaneously with the Ogo 3 data.

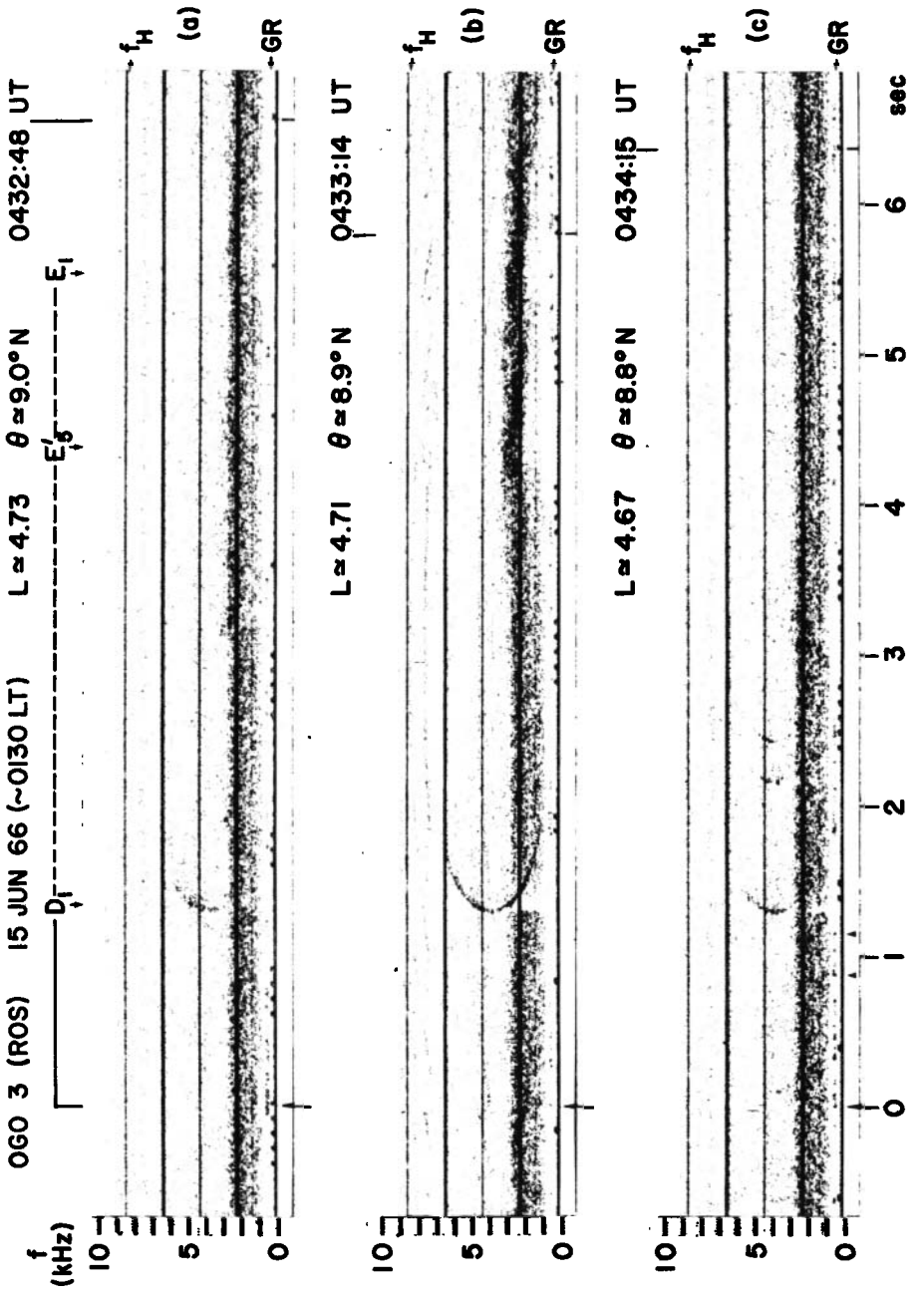

Fig. 4. Time-frequency spectrograms of whistlers received on Ogo 3 while traversing duct 1 (see Figure 2). Detailed explanation of the records is found in the text. Section *a* shows the first whistler received in this inbound pass. Section *b* shows the best defined whistler in duct 1, which extends up to ¾ of the local gyrofrequency and is followed by diffuse echoes. The noisy signal near 2.5 kHz and 6 sec (E_1) is interpreted as the echo of the ducted whistler D_1, reflected in the southern ionosphere. Still near 2.5 kHz, E_5' indicates a signal whose travel time is consistent with the mixed path echo of the whistler that propagates southward along duct 5, reflects in the ionosphere, and reaches the satellite by following duct 1 northward (see Figure 1*a*). Section *c* shows the spectra of three whistlers received when the satellite was near the inner boundary of duct 1. The arrows at the bottom indicate the times of occurrence of the corresponding causative atmospherics, which are exhibited as dots in the portion of the ground record shown at the frequency *GR*.

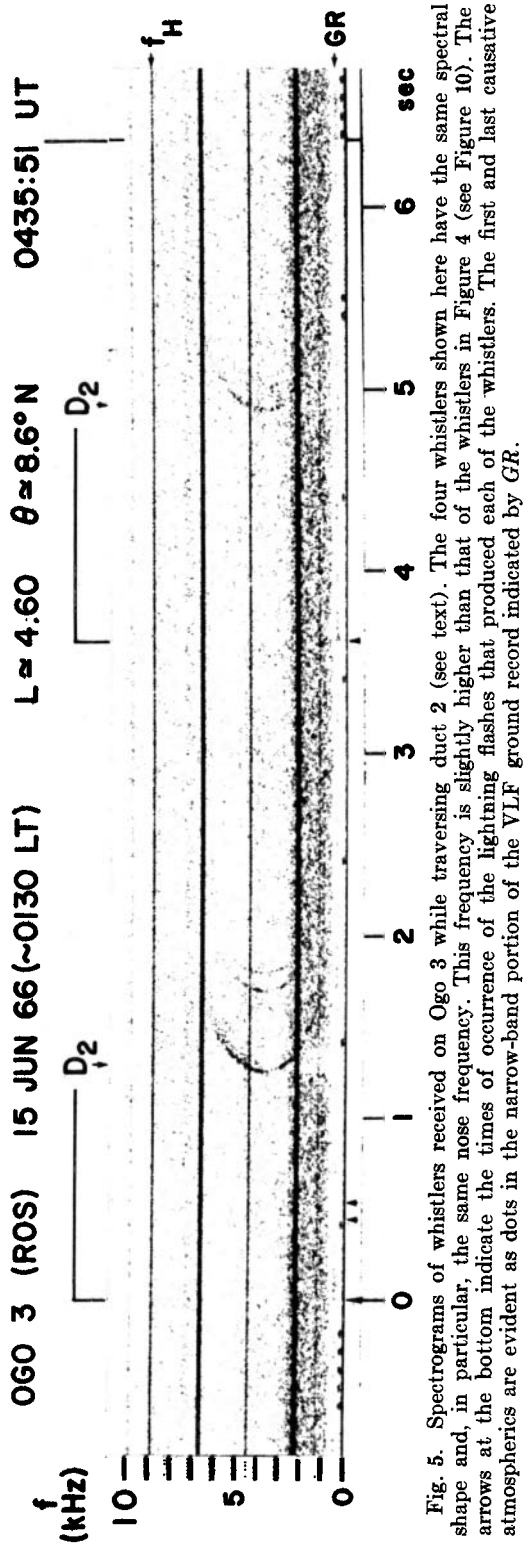

Fig. 5. Spectrograms of whistlers received on Ogo 3 while traversing duct 2 (see text). The four whistlers shown here have the same spectral shape and, in particular, the same nose frequency. This frequency is slightly higher than that of the whistlers in Figure 4 (see Figure 10). The arrows at the bottom indicate the times of occurrence of the lightning flashes that produced each of the whistlers. The first and last causative atmospherics are evident as dots in the narrow-band portion of the VLF ground record indicated by *GR*.

in this pass, at $L \cong 4.73$. This observation corresponds to the region inside the plasmapause, as shown by nearly simultaneous whistler data from Byrd Station, Antarctica (80°S, 120°W), which indicated that at the time the plasmasphere extended to at least $L = 5$. (A relatively large plasmasphere radius is consistent with the prevailing low level of magnetic activity [*Carpenter*, 1966, 1967].) Figure 4*b* shows a similar but better defined whistler, whose spectrum approaches the third horizontal line in the record, or 0.75 of the local electron gyrofrequency. Other examples of whistlers interpreted as propagating in duct 1 are shown in Figure 4*c*. Note that both the travel times and the shapes of the visible portions of the spectra are the same for all whistlers in Figure 4. (The full precision with which the dipole coordinates L and θ are given in the figures is intended to be meaningful only in locating relative, not absolute, positions.)

Figure 5 shows examples of whistlers received when the satellite was apparently traversing duct 2. Careful comparison of the whistlers in Figure 4 with those in Figure 5 shows that the latter have smaller travel times (by ~0.1 sec) and slightly higher frequency of minimum travel time (nose frequency) (see also Figure 10).

Figure 6 shows spectra received as Ogo 3 moved between ducts identified as 2 and 3. The rising tones are interpreted as leakage from the next outer duct (2) at frequencies above half the gyrofrequency, as illustrated by L_0 in the sketches of Figure 1*c* and 1*d*. (A quantitative comparison of observations and predictions based on ray tracing is presented in a later section.)

Figure 7 shows whistlers received on Ogo 3 while traversing duct 3. The nose whistlers, extending from ~2 to ~5 kHz, are interpreted as having propagated along duct 3. The higher frequency rising tones, extending from 6.2 to 7.5 kHz, are interpreted as having propagated along duct 2 up to the height where the gyrofrequency equaled twice the wave frequency and having thereafter leaked inward until they reached the satellite, as illustrated in the sketch of Figure 1*c*.

The spectrogram of Figure 8 shows VLF data received at the satellite as it traversed duct 4. Eight independent events and the corre-

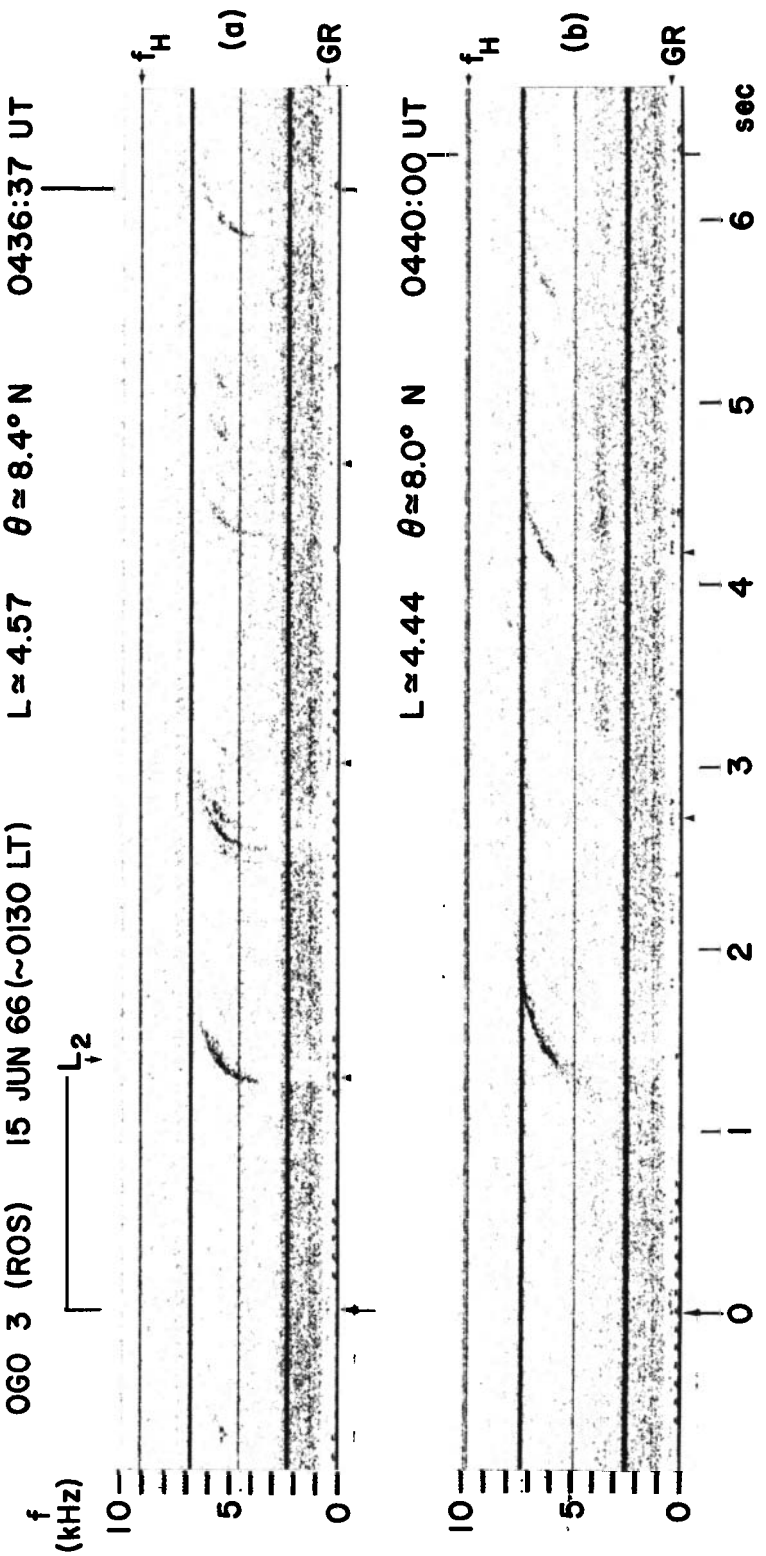

Fig. 6. Spectrograms of VLF data received on Ogo 3 between ducts 2 and 3 (see text). Only the high-frequency portions of the whistlers are observed; we here assume that they are produced by whistlers that are ducted along duct 2 and leak inward at frequencies above half the gyrofrequency (see Figures 1c and *d*). The arrows at the bottom indicate the causative atmospherics for some of the events, which are shown as dots in the ground record *GR*. At (*a*) the satellite had just crossed the inner boundary of duct 2. At (*b*) the satellite was near the outer boundary of duct 3. Accordingly, the travel times are larger than in (*a*), especially at the higher frequencies.

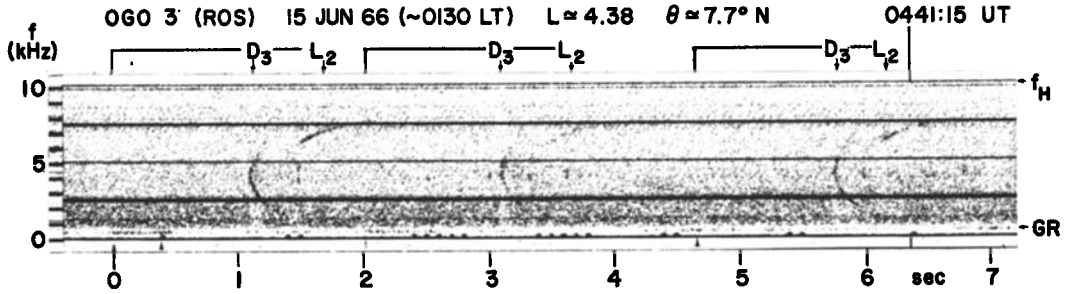

Fig. 7. Examples of VLF data received on Ogo 3 in duct 3 (see text). The arrow at the time orgin points to a portion of the lightning flash (a dot injected at frequency GR) that produced whistlers ducted along ducts 3 (D_3) and 2. A high-frequency portion of the latter leaked inward and was observed at the satellite above about 6 kHz (L_2). Three other events are seen, produced by lightning flashes near 0.3, 2.0, and 4.7 sec. The first of these only shows the whistler D_3 and not the leakage L_2.

sponding causative atmospherics are shown. The fourth and the last events exhibit leakages from two of the outer ducts (2 and 3) near 7 kHz.

Figure 9 presents data received in duct 5. The three rising tones near 8 kHz are interpreted as leakages of energy from ducts 4, 3, and 2 in the manner described in Figure 1c.

Tracings of the whistler spectra received as the satellite traversed the five ducts are superposed in Figure 10. The tracings clearly show the systematic, discrete changes of spectral shape that were observed as the satellite moved inward.

Interpretation of Data

Shape and distribution of ducts. From data of the kind shown in Figures 4 through 9, duct size and separation in L space are estimated from the corresponding lengths of time during which events characteristic of a particular duct are repeated without measurable change. Duct spread in longitude is estimated from certain features (detailed below) of both satellite and ground whistler data. The resulting descriptive model for the Ogo 3 pass is shown in Figure 11. In this figure the equatorial projection (following field lines) of the satellite orbit is shown by the dashed line, heavy portions of which represent the observed duct encounters. Estimated cross sections of the corresponding ducts are shown by the solid contours. Additional ducts are illustrated by the dashed contours, on the assumption that the ducts encountered are part of a random distribution in space. Prevailing high whistler rates of tens of events

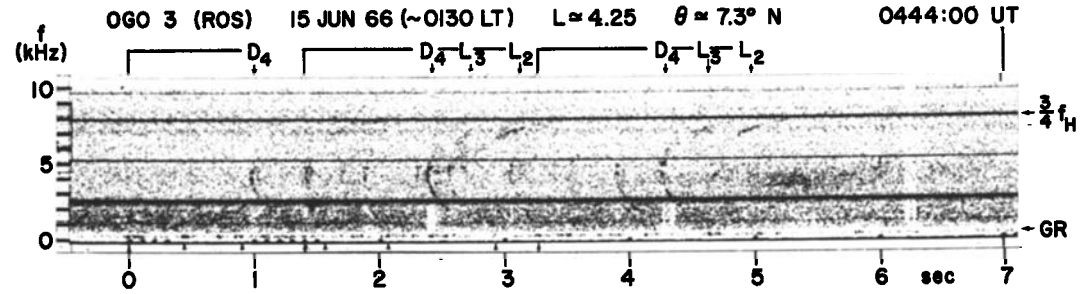

Fig. 8. Examples of VLF data received on Ogo 3 in duct 4 (see text). The arrow near 3.3 sec indicates the time of occurrence of the lightning flash that produced whistlers ducted along ducts 4 (D_4), 3, and 2. High-frequency portions of the latter two whistlers leaked inward and are shown near 7 kHz as L_3 and L_2 (see Figures 1c and d). The lightning flash near 1.4 sec produced a similar event, as indicated. The remaining components shown are whistlers ducted along duct 4, and the corresponding sources are indicated by the arrows.

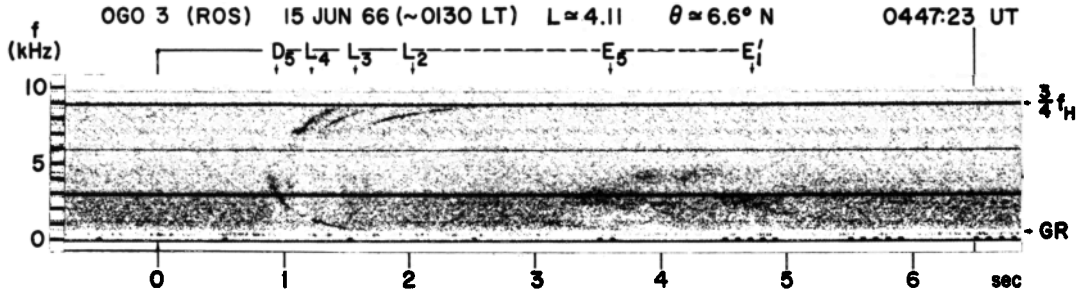

Fig. 9. VLF data received on Ogo 3 in duct 5 (see text). The arrow at the bottom indicates the time of occurrence of the lightning that produced the event shown. The whistler ducted along duct 5 is indicated by D_5, and its diffuse echo near 2.5 kHz is shown by E_5. High-frequency leakages of the whistlers ducted along ducts 4, 3, and 2 are shown by L_4, L_3, and L_2 (see Figures 1*c* and *d*). The travel time of the diffuse signal near 2.5 kHz indicated by E_1' is consistent with a mixed path echo produced by southward propagation along duct 1, reflection in the southern ionosphere, and northward propagation to the satellite along duct 5.

per minute permitted relatively precise definition of duct extent and separation in L. Table 1 (see also Figure 2) provides a summary of these dimensions expressed in terms of traversal time, corresponding distance at the equator, and corresponding distance at 300 km altitude. The thicknesses at the equator range from 223 to 430 km; at 300 km the range is 15–27 km. At the equator the effective separations between ducts range from 110 to 1140 km; at ionospheric heights the range is 6–73 km. Thicknesses and separations comparable to these were deduced from Ogo 1 whistlers received near $L = 3$ [*Smith and Angerami*, 1968].

Discussion of the duct cross section. The duct configuration of Figure 11 is based on the following arguments. The L thicknesses of the ducts cannot be much larger than those given by the duct encounters along the orbit, because appreciable overlap of ducts in L space would be inconsistent with the observations of distinct spectral shapes (compare Figures 4 and 5). Moreover, if the existing ducts were substantially wider in L than is shown in Figure 14, the satellite orbit would have to intersect them in a very particular way to yield the observed traversal times.

Elongation of the ducts in longitude by a factor of about 5 may be justified in several ways. If the ducts were substantially narrower than is shown in Figure 11 (say 2°), leakages from ducts at nearby longitudes would be expected to easily reach the satellite, following ray paths of the kind illustrated by the dotted lines emerging from ducts A and B in Figure 11 (suggestion by R. L. Smith). As the ducts are stretched in longitude, the inclination of these lines with respect to the magnetic meridian increases, thus rendering more difficult the observation of the corresponding leakages at the satellite. Although three-dimensional ray tracings including tubular ducts were not performed, it is suggested that the leakages illustrated in Figure 11 by the dotted lines (off the meridian plane by some 25°–35°) are unlikely. Therefore, since leakages from

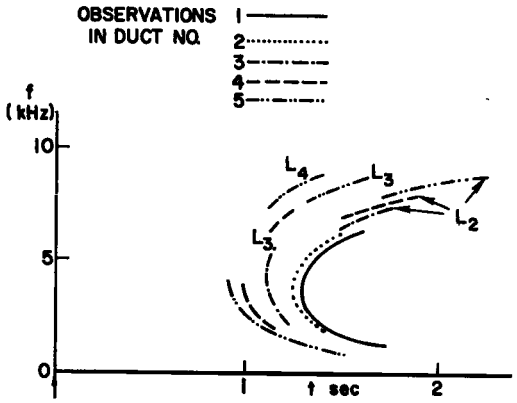

Fig. 10. Tracings of frequency-time spectra of whistlers received at Ogo 3. Observations made in each duct are shown with a different line. L_2, L_3, and L_4 denote leakages from ducts 2, 3, and 4, respectively. The tracings were done in scale, by using a common location for the causative atmospherics (time origin).

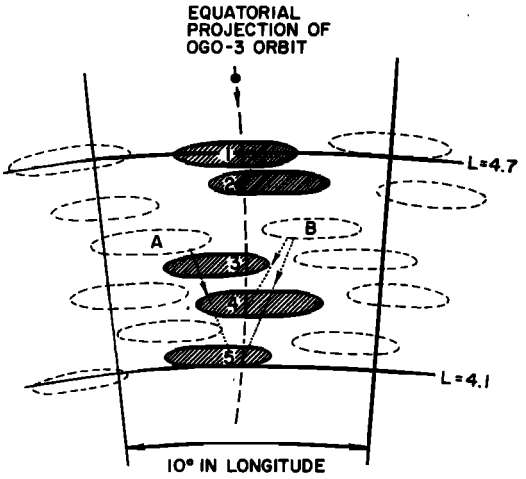

Fig. 11. Equatorial cross sections of whistler ducts. A portion of the magnetosphere 10° wide in longitude is represented in scale. The projection of the Ogo 3 satellite orbit along the magnetic field lines is shown by the dashed line, heavy portions of which indicate regions observed to be inside ducts. The dashed contours represent ducts inferred to exist, assuming that the ducts encountered by the satellite (solid contours) are part of a random distribution in space. The dotted lines represent leakages that are not observed but would be possible if the ducts were much narrower in longitude than illustrated.

the additional ducts were not observed (Figure 9, for instance, shows only leakages from ducts 2, 3, and 4 observed in duct 5), it is concluded that the duct widths cannot be much smaller than 4° in longitude.

Comparison of the present data with ground observations of whistlers indicates that the longitude widths of the whistler ducts cannot be much larger than 4°. The configuration of Figure 11 indicates that whistlers from some 40 independent ducts in the range $L = 4.1$–4.7 should be observed at Eights Station, Antarctica (75°S, 77°W), because this station can receive ducted whistlers from a sector of the magnetosphere 30° wide [*Carpenter*, 1966]. However, the satellite occurrence of whistler ducts reported here was unusually high. Furthermore, the occurrence of satellite high-frequency conjugate echoes at low L shells in the middle of June 1966 was about four times the expected value based on the occurrence in the rest of the year [Figure 7 of *Muldrew*, 1967]. If this same factor is applied to the whistler ducts, the above estimate of ground observation of ducts should drop to 10 independent ducts in the range $L = 4.1$–4.7. The number of distinct nose whistler components from a similar range of L values ($L = 4.8$–5.4, corresponding to nose frequencies between 2.1 and 3 kHz) observed at Eights (see, for instance, Figure 1 of *Angerami and Carpenter* [1966]) under conditions similar to those encountered here (nighttime, $Kp \sim 0$ for tens of hours, near 50°W longitude) is around 10 and is therefore comparable to the above estimate, if the ducts are about 4° wide in longitude. Now, if the ducts were actually wider (8°, say), the estimated number of ducts observable at the ground would decrease correspondingly (to 5, say), thus indicating that an *upper* limit for the duct widths is of the order of 4° in longitude. This upper limit is further supported by the fact that some of the ducts observed

TABLE 1. Duct Thicknesses and Separations

	Center of Duct			Effective Thicknesses			Effective Separations		
Duct	Time, UT	L, R_E	θ, °N	In Time, sec	At Equator, km	At 300 km, km	In time, sec	At Equator, km	At 300 km, km
1	04h 33m 10s	4.710	8.9	98	430	26			
							~25	110	6
2	04h 35m 46s	4.604	8.6	83	363	22			
							260	1140	73
3	04h 41m 10s	4.375	7.7	49	223	15			
							90	408	18
4	04h 43m 55s	4.259	7.3	86	389	27			
							124	560	40
5	04h 47m 17s	4.127	6.7	70	319	23			

at the satellite conceivably might not be observable at the ground, if unfavorable conditions for transmission existed in only one of the conjugate ionospheres.

Distribution of ionization along field lines. The nose frequencies of ducted whistlers on the Ogo 3 satellite lend strong support to the hydrostatic type of electron density distribution along the field lines in the *plasmasphere*, as opposed to other more rapidly varying distributions that have been proposed, such as the R^{-3}, R^{-4}, and gyrofrequency models.

The nose frequency, or frequency of minimum travel time of ducted whistlers, is related to the minimum gyrofrequency along the path by a simple proportion that depends on the ionization model used. The lightning discharges that produced the whistlers presented here were clearly identified in the VLF ground recording made at the Rosman telemetry station, which is within 2000 miles of the northern feet of the field lines passing through the satellite (see map of Figure 3). Since Ogo 3 was in the northern hemisphere, the VLF energy reached the satellite before crossing the magnetic equator ('O_+ whistlers') and the minimum gyrofrequency along the path was at the satellite (see Figure 1*a*). Therefore, in comparing different models of ionization distribution, it is meaningful to relate the nose frequency to the gyrofrequency *at* the satellite.

By using the longitudinal approximation [*Smith*, 1961] and several ionization models, the ratios of the nose frequencies of O_+ whistlers to the gyrofrequency at the satellite were calculated for several dipole latitudes θ along $L = 4.5$. The results, shown in Table 2, are applicable to the range of L values discussed here. Temperatures of 800°, 1200°, and 1600°K were taken for the diffusive equilibrium model. The ranges of values shown in each column for the diffusive equilibrium model correspond to different levels of ionization below 1000 km, yielding whistler dispersions of 3 $sec^{1/2}$ (lower values) and 4.5 $sec^{1/2}$ (higher values). These are the limits within which the ionospheric ionization generally lies. For the R^{-4} model only one value of ionospheric dispersion (3 $sec^{1/2}$) was taken, since no close comparison with the data was needed. The results in Table 2 exhibit the general trend toward higher nose frequencies for models in which the ionization increases more rapidly with distance along the path away from the point of minimum gyrofrequency [*Carpenter and Smith*, 1964].

Measurements of the nose frequencies observed in ducts 1 through 4 are shown in Table 3. The calculated and measured ratios of nose frequency of O_+ whistlers to the gyrofrequency at the satellite are plotted in Figure 12 as a function of the dipole latitude of observation. This figure shows good agreement of the data with the diffusive equilibrium model, and not with the R^{-4} model.

From these results it is concluded that whistler dispersions observed in situ in the plasmasphere are consistent with a hydrostatic distribution of electrons and the cold plasma longitudinal approximation. Such consistency lends added support to the electron density profiles determined from nose whistler data [*Angerami and Carpenter*, 1966; *Park and Carpenter*, 1970; *Park*, 1970]. Further confirmation of these results is provided by the detailed comparisons of the observations with the travel times calculated by ray tracing (see section on ray tracing analysis). These have reproduced, within a few per cent, the nose

TABLE 2. $f_n(O_+)/f_H$ (Satellite) Calculated at $L = 4.5$

	Electron Density Model			
θ	1600°K* 3.0–4.5†	1200°K* 3.0–4.5†	800°K* 3.0–4.5†	R^{-4} ~3
10°	0.424–0.430	0.432–0.438	0.439–0.445	0.508
8°	0.415–0.421	0.423–0.429	0.430–0.436	0.496
6°	0.408–0.414	0.416–0.422	0.423–0.429	0.490

* Diffusive equilibrium.
† Dispersion in the ionosphere, $sec^{1/2}$.

TABLE 3. Measured Values of $f_n(O_+)$ and f_H (Satellite)

Figure; event	L	θ, °N	$f_n(O_+)$, kHz	f_H, kHz	$f_n(O_+)/f_H$
4 *b*	4.71	8.9	3.65 ± 0.05	8.30	0.440 ± 0.006
5; 1st	4.60	8.6	3.75 ± 0.05	8.85	0.423 ± 0.006
7; 1st or 4th	4.38	7.7	4.15 ± 0.05	10.0	0.415 ± 0.005
8; 4th, 5th, or 7th	4.25	7.2	4.40 ± 0.05	10.6	0.415 ± 0.005

frequencies of the ducted whistlers and the travel times of both the ducted and leaked signals.

Estimate of enhancement factors in ducts. The electron density model to be used in the ray tracing of the next section depends on some initial calculation of enhancement factors in ducts.

First, a lower limit for the relative enhancement of density in the ducts will be derived from the data on duct size presented in Table 1. The phase refractive index μ for the whistler mode is given by [*Helliwell*, 1965]:

$$\mu^2(\psi) = \frac{f_p^2}{f(f_H \cos \psi - f)} \qquad (1)$$

where f_p is the plasma frequency ($f_p^2 = 80.6N$), f is the wave frequency, ψ is the angle between the wave normal and the geomagnetic field, and f_H is the electron gyrofrequency, proportional to the geomagnetic field strength. (N in el cm^{-3}, frequencies in kHz.)

A *necessary* condition for trapping in ducts of enhanced (or depressed) ionization is that the refractive index at zero wave normal, $\mu(0)$, has a maximum (minimum) across the duct [*Smith*, 1961], which is provided by the bump (trough) in ionization. As shown by (1), however, the decrease of f_H with radial distance tends to cause μ to increase outward, with the result that the maximum (minimum) in refractive index is shifted toward higher (lower) L values and can even disappear, depending on the relative magnitudes of the two opposing gradients.

It is therefore clear that the important feature of the electron density across the field lines is its negative gradient with radial distance. For simplicity, in the following analysis this gradient is represented by a gaussian distribution of density in L shell added to a uniform background. Such representation is appropriate in the plasmasphere, because in this region the background ionization decreases slowly with radial distance (see Figure 2 of *Angerami and Carpenter* [1966] or the profile of Figure 16, determined from the present data), thus leading to minor corrections for the radial density gradients. We therefore consider a field-aligned duct defined by:

$$N(L) = N_o \cdot \left\{1 + C \cdot \exp \frac{-(L - L_o)^2}{2 \cdot \Delta L^2}\right\} \qquad (2)$$

where N_o is the background density (N at $|L - L_o| \gg \Delta L$), C is the relative increase (or depression, if negative) of density at the center of the duct ($L = L_o$), and ΔL repre-

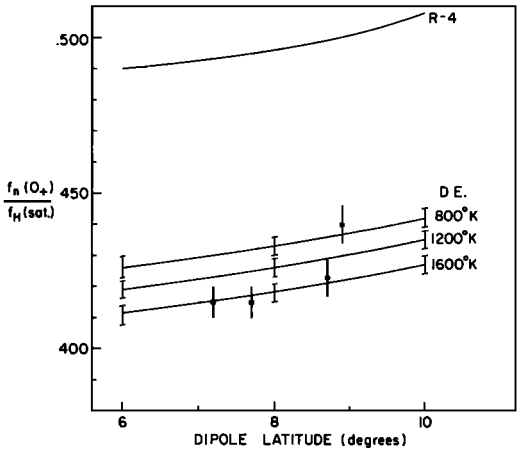

Fig. 12. Ratios of nose frequency of O_+ whistlers to gyrofrequency at the satellite, plotted as a function of the spacecraft latitude. The thin lines show values calculated at $L = 4.5$ for the R^{-4} and diffusive equilibrium models. For the latter, three different temperatures were used, and the associated vertical bars correspond to ionospheric dispersions of 3.0 sec$^{1/2}$ (lower values) and 4.5 sec$^{1/2}$ (higher values). The experimental data are shown by heavy dots that, from left to right, correspond to nose whistlers observed in ducts 4, 3, 2, and 1. The associated vertical bars represent uncertainty in measurement of the nose frequencies.

sents the duct semithickness in L space, which are shown in Table 5, in agreement with the ducts of Table 1. It can be easily shown that the longitudinal refractive index, $\mu\ \psi = 0$), at a frequency f has a maximum (or minimum, if $C < 0$) across the duct at latitude θ only if

$$|C| > \frac{4.95 \cdot \Delta L \cdot F(\theta)}{L_o \cdot (1 - f/f_H) \pm 3 \cdot \Delta L \cdot F(\theta)} \qquad (3)$$

where f_H is the local electron gyrofrequency, the minus sign in the denominator is applicable to enhancements (the plus sign to troughs, $C < 0$), and $F(\theta)$ is a decreasing function of latitude given by

$$F(\theta) = \frac{1 - \sin^4 \theta}{(1 + 3 \sin^2 \theta)^2} \qquad (4)$$

It is clear from (3) and (4) that the most unfavorable condition for trapping waves at a given frequency takes place at the equator, where f_H reaches a minimum ($=f_{H0}$), and $F(\theta)$ is maximum, thus leading to a maximum value for $|C|$.

It is also seen from (3) that the smallest enhancement C needed to trap a wave across the equatorial plane is approximately proportional to the duct thickness (ΔL), is inversely proportional to the L value at the duct (L_o), and increases with the normalized wave frequency at the equatorial crossing (f/f_{Ho}). In particular, the minimum enhancement needed to trap a frequency equal to half the minimum gyrofrequency is about twice that needed to trap much lower frequencies.

By using the observed values of ΔL and L_t of Table 1 (see Table 5), minimum enhancements needed to trap different frequencies across the equatorial plane along each of the observed ducts were calculated from equation 3 with $F(\theta) = 1$. The results are shown in Table 4 and indicate that the average enhancement in a 'whistler duct' must be at least 3.2% to trap the lower frequencies, and that a duct with enhancement less than about 6.4% cannot support guided whistlers extending up to the 'duct cutoff' at half the minimum gyrofrequency.

An upper limit for whistler duct enhancements may be inferred by recalling that electron density equatorial profiles obtained from ground nose whistlers are in general smooth;

TABLE 4. Lower Limit of Enhancements Needed for Trapping

Duct	% Enhancements Needed to Guide Frequency f Across the Equatorial Plane	
	$f/f_{H0} \ll 1$	$f/f_{H0} \sim 0.5$
1	3.8	7.7
2	3.2	6.4
3	2.1	4.2
4	3.6	7.3
5	3.1	6.2
Median	3.2	6.4

variations of density between neighboring points at a given time and longitude are in general less than 15% and rarely exceed 25% [cf. *Angerami and Carpenter*, 1966]. Since the existing ducts have probably random distribution of enhancements, those with enhancements above about 6% being observed, one concludes that the density enhancements in whistler ducts generally lie between 6% and 22% and rarely exceed 33%.

Unfortunately, during the time interval that these data were taken, Ogo 3 was in the 'accelerated sub-com' telemetry mode, and no simultaneous PCM data from other experiments are available for correlations. Therefore, no comparisons of the densities inferred from the present analysis can be made with direct probe measurements. It is hoped that such comparisons can be made in the future by using other passes of Ogo 3, despite the constraints imposed on probe measurements by the high resolutions needed in time and density (probably better than 10 sec and 3%, respectively).

Ray Tracing Analysis Based on the Ogo 3 Data

A ray tracing analysis has shown consistency between the spectra illustrated in Figures 4 through 9 and a propagation model of the magnetosphere that includes: (1) ducts with the L thicknesses and positions shown in Figure 11; (2) ducts of enhanced ionization (see later discussion); and (3) use of a diffusive equilibrium model of the fieldline distribution of ionization. The model magnetosphere used in the computations is described in the appendix.

Figure 13 illustrates the predicted behavior

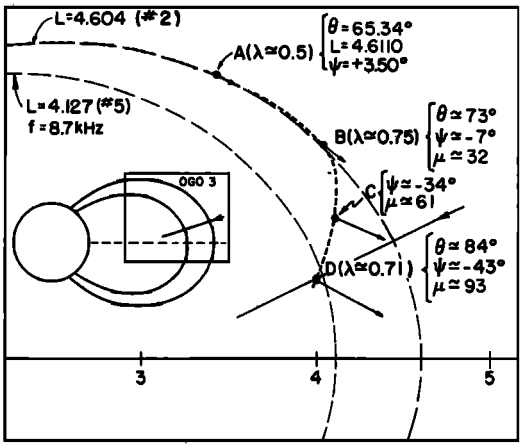

Fig. 13. Ray tracing to explain leakage from duct 2, as observed in duct 5. The frequency is 8.7 kHz, corresponding to the top of component L_2 in Figure 9. The model magnetosphere is described in the appendix. Initial conditions were chosen at point A in such a way that the ray intercepts the satellite at point D. Beyond point B the wave normal angle and the ratio of wave frequency to local gyrofrequency are large, favoring Landau damping. Nevertheless, the wave was observed at the satellite (Figure 9). The ray was also traced backward to reproduce the complete propagation path, part of which is shown.

of a wave packet propagating upward along a duct at $L \sim 4.6$. As long as the gyfrofrequency is higher than twice the wave frequency, the wave normals are constrained to lie inside a cone around the magnetic field, and the packet follows a snakelike path along the duct. Beyond point A, where the gyrofrequency is nearly twice the wave frequency ($\lambda = f/f_H \cong 0.5$), the wave normals tend to turn outward with respect to the direction of the local magnetic field, and the energy is no longer trapped. In spite of the increasing wave normal angle ψ (arrows represent the refractive indices μ in the wave normal direction), the packet remains near the duct for an appreciable distance. Then near some point B the ray direction begins to change rapidly and the ray turns inward, providing an inward 'leakage.'

In point of detail, the ray path of Figure 13 represents a wave packet that originated in duct 2 (see Figures 2 and 11) and was observed on Ogo 3 in duct 5 (point D in Figure 13). The frequency is 8.7 kHz, corresponding to the upper end of signal L_2 in the spectrum of Figure 9. (Further details of this case appear below and in Table 5.)

The geometrical shapes of the ray paths in the untrapped region (beyond the point where $\lambda = 0.5$) are a function of the wave normal angle at the untrapping point (see next subsection). This is illustrated in Figure 14*a* and *b* by two ray paths, each beginning in duct 1 at frequency 6.1 kHz but having different wave normal angles at the untrapping point (A in 14*a*, D in 14*b*). In Figure 14*a* the wave normal angle at A is $-6.33°$; in Figure 14*b* it is $+6.0°$ at D (see Figure 15 for coordinates). In 14*a* the ray soon leaves the vicinity of the duct and leaks inward so as to intercept the Ogo 3 orbit at a lower altitude. In Figure 14*b*, with a small positive wave normal angle at the untrapping point, the wave-packet remains 'in' the duct over a relatively great distance, intercepting the satellite at point F and only leaving the duct at point G. The latter ray path corresponds to the highest frequency observed in the ducted whistler of Figure 4*b*.

Travel time calculations were made for the highest whistler frequencies received in certain ducts and the lowest and highest frequencies in various leakage signals. Through adjustments of the initial conditions at the untrapping point, rays were found that could intercept the satellite in a manner consistent with the observations. For example, the ray of 14*b* corresponds to the highest frequency observed from Ogo 3 in duct 1 (see Figure 4*b*). The ray shown in Figure 13, at 8.7 kHz, corresponds to the highest frequency in the leakage L_2 of Figure 9. Further examples of comparisons of calculations and data are given in Table 5. (The initial conditions listed in Table 5 are such that, when the rays are traced back down the ducts to ionospheric heights, the input wave normals are near the vertical, as they should be following excitation of the whistler mode from below.) The range of values in the column of observed travel times represents the estimated uncertainties in measurement, which are mainly caused by the steep slope of travel time versus frequency in the corresponding data. The good agreement of the calculated travel times with the observations indicates that the behavior of untrapped ray paths can be closely predicted by ray tracings in a model magnetosphere.

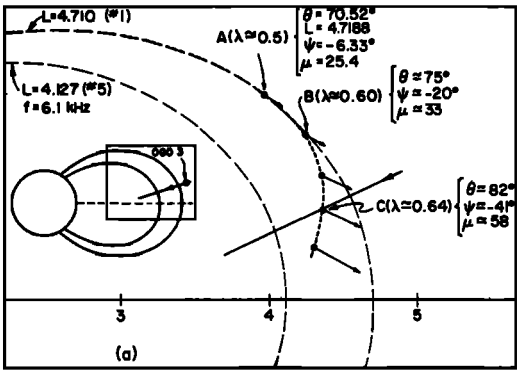

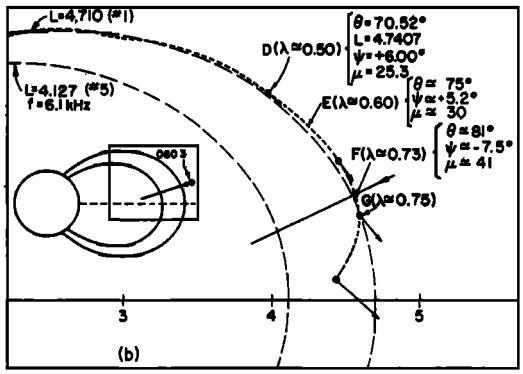

Fig. 14. Meridian cross sections of the magnetosphere showing ducts 1 and 5 and a portion of the Ogo 3 orbit. The dashed lines indicate ray paths for a frequency of 6.1 kHz trapped in duct 1. The arrows along the rays indicate the wave normal directions, and their lengths are proportional to the refractive indices μ. Section a: at $A(\lambda \cong 0.5;\ L \cong 4.719)$ the wave normal points outward ($\psi \cong 6.3°$). Beyond this point the wave normal turns counter-clockwise with respect to the local magnetic field, and the wave packet crosses the center of the duct ($L = 4.71$) at B, with a relatively large wave normal angle ($\psi \cong -20°$). Section b: in order that the ray reach the satellite at F and explain the highest frequency observed in the ducted whistler of Figure 4b, different conditions were chosen at point D ($\lambda \cong 0.5$; $L \cong 4.741$; wave normal pointing inward, $\psi \cong +6.0°$). Beyond this point the wave normal turns counter-clockwise with respect to the local magnetic field, as it did in (a). The computed travel time of 1.53 sec agrees well with the one measured in Figure 4b (1.50 ± 0.03 sec). A satellite at G could observe a frequency of ¾ of the local gyrofrequency.

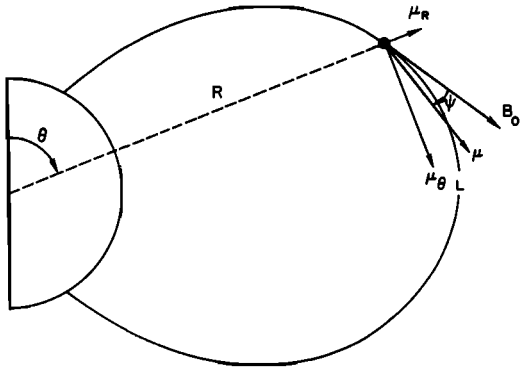

Fig. 15. Coordinate systems used in the ray tracings. The symbol ψ is the angle between the magnetic field direction (B_0) and the wave normal, and μ is the refractive index.

Remarks on the question of propagation in ducts of depressed or enhanced ionization. It has been found possible to predict the observed properties of the data by using a magnetospheric model involving ducts of enhanced ionization. It remains to be shown that similar effects could not be achieved in depressions of ionization. *Smith* [1961] has shown that ducting along ducts of depressed ionization is possible even at frequencies above half the gyrofrequency. However, leakage from such ducts is also expected because, as was shown in the preceding section, the maximum (or in the present case the minimum) in the refractive index across a duct disappears if the condition (3) is not satisfied. In other words, the duct effectively disappears as the gyrofrequency is approached ($f/f_H \rightarrow 1$). Beyond this point the gradient of refractive index is directed away from the earth due to the predominance of f_H in the denominator of (1), and therefore the wave normal rotates outward. Since the wave packet velocity is normal to the refractive index surface, which is chalice-shaped for frequencies larger than $f_H/2$, it follows that the energy will ultimately leak inward from either troughs or ducts of enhanced ionization. The choice of enhancements therefore must be based on more quantitative characteristics of the leakages. To this end, ray tracings (see previous section) were performed both for the enhancements C_4 given in Table 3 and for depressions of ionization (by taking the negative of C_4). The calculated travel times agreed very well with the observations (see Table 2)

TABLE 5. Examples of Comparison of Calculated and Observed Travel Times for Whistlers Involving a Portion of Unducted Path

Frequency, kHz	Initial Conditions			Total Travel Times	
	L	θ	ψ	Calculated	Observed
6.1*	4.7407	70.52°	6.00°	1.53	1.50 ± 0.03
6.1†	4.6190	71.96°	−0.25°	1.36	1.32 ±0.02
7.7‡	4.6139	67.80°	−6.89°	1.69	1.65 ± 0.05
8.7§	4.6110	65.34	3.50°	2.30	2.2 ± 0.1

* Highest frequency observed in duct 1 near 04h 33m 10s; see Figure 4*b*. Ray tracing in Figure 14*b*.
† Highest frequency in the leakage from duct 2, observed between ducts 1 and 3 near 04h 37m 30s.
‡ Lowest frequency in the leakage from duct 2, observed in duct 5 near 04h 46m 20s, cf. Figure 9.
§ Highest frequency in the leakage from duct 2, observed in duct 5 near 04h 48m 15s, cf. Figure 9. Ray tracing in Figure 13.

when enhancements were assumed, but not in the case of troughs. In the latter case, the predicted frequencies of the leakages were much higher than the actual observations. It was also found that, although the wave normals at ionospheric heights were favorable for penetration (nearly vertical) in the case of enhancements, they were close to the resonance cone in the case of troughs and were therefore unfavorable for penetration. This is actually one of the arguments given by *Smith* [1961] in favor of trapping in enhancements as opposed to troughs.

Finally, it may be shown that leakages from troughs of ionization could explain the observations only if the depression factors (negative C_i in equation 3) had very particular values so that the troughs effectively disappear near $f/f_H = 0.5$.

Remarks on the amplitudes of the unducted signals. A casual thought about the leakage from ducts might lead to the conclusion that after being untrapped the signals would attenuate rapidly due to strong divergence of the rays. However, further consideration suggests that the divergence of the leaked rays should be restricted due to the high anisotropy of the medium in the unducted portions of the paths, where the wave frequency is greater than half the local electron gyrofrequency [e.g., *Helliwell*, 1965]. Such expectation has been confirmed by ray tracing results and by the experimental data. For instance, several ray paths of 8.7-kHz signals from duct 2 were calculated by using widely different initial conditions which, although admittedly not exhaustive, are probably representative of the actual range of possibilities. These calculated ray paths were distinct but nevertheless confined to a width of $\sim 0.14\ R_E$ near their intersection with the satellite orbit. As another example, the separation between the rays of Figure 14*a* and *b* near the satellite orbit is $\sim 0.20\ R_E$.

Even more significantly, a detailed analysis of the data showed that the leakages from a particular duct at a given frequency are indeed observed only over a limited portion of the satellite orbit. As a typical example, the leakages L_2 from duct 2 at 7.7 kHz were observed only from 04h41m04s to 04h46m20s UT, over a distance of 0.17 R_E along the satellite orbit. Since ray tracings (similar to that shown in Figure 13) showed that the corresponding rays intercept the orbit at ~45°, it follows that the tube of rays L_2 at 7.7 kHz is about 0.12-R_E wide in the meridian plane. Because this dimension is about twice the thickness of duct 2 (cf. Table 1) and assuming that the ducts are much wider in longitude than in L (Figure 11), the expected attenuation due to spreading is only 3 db.

The spectra of Figures 4 through 9 indicate that the average intensities of leaked signals and ducted whistlers are in general comparable, in agreement with the limited attenuation due to spreading. It is therefore apparent that amplification mechanisms are *not needed* to explain the observed relative amplitudes in

this case study. However, one cannot necessarily infer that no amplification and/or damping takes place (see next subsection).

A much more detailed study of the amplitudes is not warranted at this stage for the following reasons. First, owing to the log compression and limiting already mentioned, the broadband spectra yield only relative amplitudes; and absolute measurements of amplitude (in digital form) from the same experiment were not available because the spacecraft was at the time in 'accelerated sub-com mode.' (Accordingly, no simultaneous digital data from other experiments on Ogo 3 are available for correlations.) Second, as the darkness of the spectra indicates, there is much more variation in amplitude from event to event than among different components in the same event. This invalidates accurate comparisons between, for example, the amplitude of D_2 in Figure 5 and the amplitudes of L_2 values in the subsequent figures. Finally, one cannot rule out a priori the effect of the source location on the relative amplitudes of signals excited in different ducts. For example, it is difficult to interpret the differences in amplitude among the various components in one event, such as in Figure 9.

Remarks on the low- and high-intensity cutoffs of the observed spectra. The high and low cutoff frequencies of the observed spectra, if not attributable to the spectrum of the lightning source, may conceivably be due to either inaccessibility or thermal damping. (Limitation due to the lightning sources can be disregarded by observing that distinct components produced by the same source cover different frequency ranges, and that in events with wide frequency coverage there is a systematic latitude change in the cutoffs of a given component.) Sufficiently comprehensive ray tracing analysis has not been attempted to establish conditions of accessibility.

It appears likely, however, that accessibility is the controlling factor in some of the low-frequency cutoffs. This may be seen qualitatively from the ray tracings. For the satellite at a given position, and observing leakage from an outlying duct, successively lower frequencies will reach the untrapping condition at points successively closer to the equator, with frequencies below the half minimum gyrofrequency $f_{H0}/2$ not being untrapped at all. In some range of frequencies above the half minimum gyrofrequency, the portions of the magnetosphere illuminated by unducted rays will be somewhat restricted and may not include the position of the satellite. The sharp low cutoff in some of the leakages (e.g., Figure 9) is also suggestive of the behavior of the amplitude near a caustic, in a manner similar to what happens at the 'skip distance' in HF communications.

On the other hand, it seems unlikely that a combination of cyclotron amplification and Landau damping can be responsible for the low cutoff of the leakages, since both effects are expected to produce only larger amplitudes at lower frequencies. Indeed, ray tracings of leakages from one duct to a given satellite position show that for lower frequencies both f/f_H and the wave normal angles are smaller in a substantial portion of the ray paths. Furthermore, *Liemohn's* [1967] calculation of cyclotron attenuation of parallel whistler-mode waves in the presence of a loss-cone distribution of ~1-kev electrons (see his Figure 7) indicates that low values of f/f_H favor amplification. Also, *Kennel and Thorne's* [1967] results showed that, at least for $f/f_H \ll 1$, the Landau damping varies directly with the wave normal angle.

The above discussion qualitatively indicates that both cyclotron resonance amplification and Landau damping may play a role in the upper cutoff of the satellite-observed whistlers, with the first providing smaller amplification as the frequency is raised [*Liemohn*, 1967], and the second more strongly attenuating the signals with larger wave normal angles [*Kennel and Thorne*, 1967]. The ray path of Figure 13 shows the typical tendency of the wave normal to approach the resonance condition after untrapping; the angle between the wave normal and the resonance direction decreases from 9° at point C to 2° at D (ψ at resonance $= \cos^{-1} \lambda$) and then rapidly falls below 1°. The travel times also increase accordingly; both effects are more pronounced at higher frequencies. (This travel time dependence on frequency is exhibited by the large dispersion near the upper cutoffs of leakages, e.g., Figure 9.) Such behavior suggests that the untrapped waves will ultimately be attenuated, probably

by Landau damping, consistently with the lack of observation of signals identifiable as leakages at ionospheric altitudes. The Ogo broadband receivers, with an upper cutoff at 12.5 kHz, can only detect leakages that untrap from ducts beyond 3.3 R_E, corresponding to $f_H \cong 25$ kHz. Although this leaves a relatively small region able to generate observable leakages once the plasmapause at a typical $L \sim 4$ is considered, their occurrence together with ducted whistlers is not uncommon.

The relative contributions to the upper cutoff of cyclotron resonance, Landau damping, and accessibility remain to be assessed. For such a detailed comparison the published cyclotron and Landau damping rates must be recalculated to include actual conditions along the rays. The typical ray path for frequencies near the upper cutoff of a leakage (Figure 13) shows that in the portion AB the value of λ $(=f/f_H)$ varies from 0.5 to 0.75 (corresponding to $f/f_{H0} \cong 1.06$), and the wave normal angle (ψ) from 3.5° to −7°. Therefore, *Liemohn's* [1967] cyclotron calculations must be extended to include $f/f_{H0} \cong 1.06$ at latitudes greater than ~15°, and to account for propagation at small but non-zero angles with the magnetic field. The Landau damping calculations of *Kennel and Thorne* [1967] must also be extended to include values of $\lambda \cong 0.7$ (as in *BD*, Figure 13), since their reported results are for low frequencies only ($\lambda = f/f_H \ll 1$).

Although the upper cutoff of satellite-observed whistlers may be in part due to thermal effects, this is not true for ground observations. Indeed, by confirming that the whistler ducts are enhancements and that wave packets actually untrap as expected at frequencies above half the electron gyrofrequency, the present study clearly establishes that the observed upper cutoff of ground whistlers near $f_{H0}/2$ is the 'duct cutoff,' a cold plasma propagation effect, since higher frequencies would be untrapped in crossing the equatorial plane.

Summary and Conclusions

Whistlers received by the Stanford University/Stanford Research Institute broadband (0.3–12.5 kHz) VLF receiver aboard Ogo 3 in the inbound pass of June 15, 1966, provided the most complete evidence for whistler ducts known to date. Five discrete whistler ducts were intersected between $L = 4.7$ and 4.1, each duct being characterized by reception at the satellite of ducted nose whistlers with distinct spectral shapes, along with high-frequency portions of whistlers that propagated inward from the outer ducts (leakages). Analysis of the data yielded several physical characteristics of the ducts observed (sizes, separations, shapes, and relative enhancements), experimental confirmation of predicted properties of ducted propagation (inward leakages with limited spreading and high amplitudes, duct cutoff, and validity of longitudinal approximation), evidence for the hydrostatic type of field line distribution of ionizaton in the plasmasphere, and renewed confidence in results of ray tracing.

The L shell thicknesses of the observed ducts ranged between 0.035 and 0.070 R_E, corresponding to spans of 220 to 430 km radially at the equator, or 15 to 26 km on the meridian plane in the ionosphere. The L shell interduct separations, identified by the interval between observations of successive nose whistlers exhibiting distinct spectral shapes, ranged from 110 to 1140 km radially at the equator, corresponding to north-south separations of 6 to 73 km in the ionosphere. The width of the observed ducts in longitude was estimated at about 4°, thus implying east–west elongated equatorial cross sections by factors of 4 to 8. It was shown that a minimum relative enhancement of density in a duct is needed if waves at frequencies up to half the minimum gyrofrequency are to remain trapped across the equator. The estimated minimum enhancements ranged between 4% and 8% for the ducts observed. Less pronounced bumps of ionization are predicted to produce ground whistlers with upper cutoffs that are proportionately lower, which finally approach zero frequency as the enhancement is decreased to half the above values.

The travel times of the observed leakages from the outer ducts were reproduced within a few per cent by ray tracing in a model magnetosphere that included ducts of enhanced ionization, thus lending renewed confidence in the ability of ray tracing to predict the behavior of nonducted waves in the magnetosphere. The fact that no agreement could be reached when troughs of depressed ionization were used in the model is new evidence that the

whistler ducts are indeed enhancements.

The in situ verification that the whistler ducts are enhancements and that wave packets at frequencies above half the electron gyrofrequency are actually untrapped clearly shows that the upper cutoff of ground-observed whistlers near $f_{H0}/2$ is the duct cutoff, a cold plasma propagation effect.

Ray tracings for the leakages show a limited spreading of the energy after the wave packet is untrapped, a predictable behavior due to the strong anisotropy of the medium at frequencies above half the electron gyrofrequency. This result is consistent both with the range of observation of the leakages, which imply a twofold enlargement in the cross section of the tube of rays, and with the large amplitudes of the observed leakages.

The low-frequency cutoffs of the leakages are probably due to accessibility, since known warm plasma effects favor smaller attenuation at the lower frequencies. Cyclotron resonance and Landau interactions may play a role (not yet fully assessed) in the explanation of the upper cutoff of the leakages, since the corresponding conditions (large values of f/f_H and wave normal angle) favor attenuation.

The observed travel times and frequencies of minimum travel time of ducted whistlers agree within a few per cent with the values calculated in the hydrostatically supported model magnetosphere either by ray tracing or by the strictly longitudinal approximation. It is therefore concluded that the hydrostatic type of electron density distribution along field lines is applicable in the plasmasphere, and that the strictly longitudinal approximation is valid for the great majority of ground whistlers (ducted). These facts add confidence in results based on analysis of ground whistlers, such as electron densities and convective motions.

Appendix: Ray Tracing

The ray tracings were performed by a Fortran H program written for the IBM 390/67 computer by *Walter* [1969]; it is similar to that developed by *Kimura* [1966].

The geomagnetic field model used was a centered dipole with electron gyrofrequency of 791 kHz at the ground on the equator, chosen to match the gyrofrequencies measured by the rubidium vapor magnetometer aboard Ogo 3 in the region of interest.

TABLE 6. Duct Parameters Used in the Ray Tracings

Duct	C_i	L_i	ΔL_i
1	0.10	4.710	0.0353
2	0.16	4.604	0.0290
3	0.17	4.375	0.0180
4	0.10	4.259	0.0300
5	0.10	4.127	0.0250

The electron and ion densities above 1000 km were represented by a field-aligned isothermal diffusive equilibrium (DE) model at 1000°K [*Angerami and Thomas*, 1964]. At 1000 km the composition was taken as 80% of H^+ and 20% of O^+, and a density of 2800 electrons cm^{-3} was chosen to reproduce the travel time observed at the nose of duct 1. The effect of the ionization below 1000 km was accounted for by a constant dispersion $D = 3\ \text{sec}^{1/2}$ ($D = t \cdot f^{1/2}$).

The ducts were represented by field-aligned enhancements of ionization obtained by multiplying the densities given by the *DE* model, N_{DE}, by a product of bell-shaped functions of L for each duct:

$$N_{DE} \cdot \prod_{i=1}^{m} \left\{1 + C_i \cdot \exp\left(\frac{-(L - L_i)^2}{2 \cdot \Delta L_i^2}\right)\right\} \quad (5)$$

where

m, = number of ducts (5)
C_i, = enhancement at ith duct (negative for troughs of ionization)
L, = local L value
L_i, = L value at center of ith duct
ΔL_i, = semiwidth of ith duct, at inflection points

The values of L_i and ΔL_i (Table 6) were chosen in agreement with the observations shown in Table 1. The values of the enhancements C_i shown in Table 6 are such that the travel times calculated by the strictly longitudinal approximation (or by actual ray tracing) match those observed near the nose frequency in each duct. The minimum enhancement of 10% was chosen somewhat above the higher figures of Table 4, on the assumption that any of the ducts could support trapped propagation at half the gyrofrequency across the equatorial plane. The continuous line of

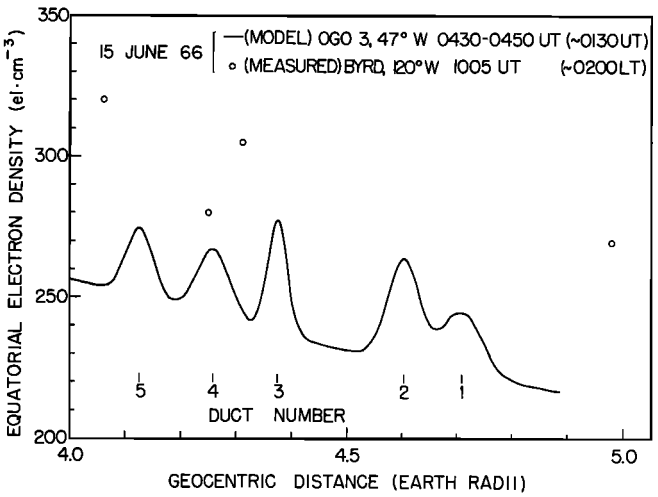

Fig. 16. Electron density in the equatorial plane. The solid line represents the model used in the ray tracings, which has been adjusted to match the travel times of ducted whistlers observed in each of the five ducts. The vertical scale is very expanded to show the 10% enhancements. The open circles are densities determined from nose whistlers recorded at Byrd Station, Antarctica, within 6 hours but at approximately the same local time as the Ogo 3 data. The nearly 20% difference between the densities seen at the Byrd and Ogo 3 meridians is attributed to a longitude effect.

Figure 16 shows the equatorial electron density for the model. The vertical scale is expanded to show clearly the enhancements in the ducts. In the same plot the open circles represent equatorial electron densities determined from nose whistlers recorded at Byrd Station, Antarctica (120°W, 80°S), about 60° west of Ogo 3 but approximately at the same local time as the satellite data described here. (The nearly 20% higher densities in the Byrd meridian are attributed to the longitude effect.)

Acknowledgments. I am indebted to R. A. Helliwell, D. L. Carpenter, R. L. Smith, T. F. Bell, and H. B. Liemohn for useful discussions and helpful criticisms on the manuscript; to J. Katsufrakis for calling attention to interesting data; to F. Walter for making available his ray tracing computer program before publication; and to J. Heppner for providing magnetometer data acquired on Ogo 3.

The research for this work was sponsored in part by the National Aeronautics and Space Administration under contract NAS 5-2131 and grants NGR 05-020-288 and NGL 05-020-008; in part by the National Science Foundation, Office of Antarctic Programs, under grant GA-1151; and in part by the National Science Foundation, Office of Computer Sciences, under grant NSF GP-948.

The Editor wishes to thank J. A. Fejer and H. B. Liemohn for their assistance in evaluating this paper.

References

Angerami, J. J., A whistler study of the distribution of thermal electrons in the magnetosphere, *Tech. Rep. SU-SEL-66-017*, Radiosci. Lab., Stanford Electronics Labs., 1966.

Angerami, J. J., and D. L. Carpenter, Whistler studies of the plasmapause in the magnetosphere, 2. Electron density and total tube content near the knee in magnetospheric ionization, *J. Geophys. Res., 71*, 711, 1966.

Angerami, J. J., and J. O. Thomas, Studies of planetary atmospheres, 1, The distribution of electrons and ions in the earth's exosphere, *J. Geophys. Res., 69*, 4537, 1964.

Carpenter, D. L., Whistler studies of the plasmapause in the magnetosphere, 1, Temporal variations in the position of the knee and some evidence on plasma motions near the knee, *J. Geophys. Res., 71*, 693, 1966.

Carpenter, D. L., Relations between the dawn minimum in the equatorial radius of the plasmapause and *Dst*, *Kp*, and local *K* at Byrd Station, *J. Geophys. Res., 72*, 2969, 1967.

Carpenter, D. L., Ducted whistler-mode propagation in the magnetosphere; a half-gyrofrequency upper intensity cutoff and some associated wave growth phenomena, *J. Geophys. Res., 73*, 2919, 1968.

Carpenter, D. L., and R. L. Smith, Whistler measurements of electron density in the magnetosphere, *Rev. Geophys., 2,* 415, 1964.

Cerisier, J. C., Accessibilite par propagation aux resonances tres basse frequence dans l'ionosphere, *Ann. Geophys., 23,* 249, 1967.

Helliwell, R. A., *Whistlers and Related Ionospheric Phenomena,* Stanford University Press, Palo Alto, Calif., 1965.

Jensen, D. C., and J. C. Cain, An interim geomagnetic field, *J. Geophys. Res., 67,* 3568, 1962.

Kennel, C. F. and R. M. Thorne, Unstable growth of unducted whistlers propagating at an angle to the geomagnetic field, *J. Geophys. Res., 72,* 871, 1967.

Kimura, I., Effects of ions on whistler-mode ray tracing, *Radio Sci., 1,* 269, 1966.

Liemohn, H. B., Cyclotron-resonance amplification of VLF and ULF whistlers, *J. Geophys. Res., 72,* 39, 1967.

Liemohn, H. B., and F. L. Scarf, Whistler determination of electron energy and density distributions in the magnetosphere, *J. Geophys. Res., 69,* 883, 1964.

Muldrew, D. B., Medium frequency conjugate echoes observed on topside-sounder data, *Can. J. Phys., 45,* 3935, 1967.

Park, C. G., Whistler observations of the interchange of ionization between the ionosphere and the protonosphere, *J. Geophys. Res., 75*(22), 1970.

Park, C. G., and D. L. Carpenter, Whistler evidence of large scale electron density irregularities in the plasmasphere, *J. Geophys. Res., 75*(19), 3825, 1970.

Rorden, L. H., L. E. Orsak, B. P. Ficklin, and R. H. Stehle, Instruments for the Stanford University/Stanford Research Institute VLF experiment (4917) on the EOGO satellite, *SRI Rep.,* Stanford Res. Institute, 1966.

Smith, R. L., Propagation characteristics of whistlers trapped in field-aligned columns of enhanced ionization, *J. Geophys. Res., 66,* 3699, 1961.

Smith, R. L., and J. J. Angerami, Magnetospheric properties deduced from Ogo 1 observations of ducted and nonducted whistlers, *J. Geophys. Res., 73,* 1, 1968.

Walter, F., Nonducted VLF propagation in the magnetosphere, *Tech. Rep. Radiosci. Lab.,* Stanford Electronics Labs., 1969.

(Received August 12, 1969;
revised May 27, 1970.)